

# Observation of a chirality created exchange bias effect

K. Chen,<sup>1,\*</sup> A. Philippi-Kobs,<sup>2</sup> V. Lauter,<sup>3</sup> A. Vorobiev,<sup>4</sup>  
E. Dyadkina,<sup>5</sup> V. Yu. Yakovchuk,<sup>6</sup> S. Stolyar,<sup>6,7</sup> and D. Lott<sup>8</sup>

<sup>1</sup>*Helmholtz-Zentrum Berlin für Materialien und Energie,  
Albert-Einstein-Strasse 15, 12489, Berlin, Germany*

<sup>2</sup>*Deutsches Elektronen-Synchrotron (DESY), Notkestrasse 85, 22607 Hamburg, Germany*

<sup>3</sup>*Neutron Scattering Division, Neutron Sciences Directorate,  
Oak Ridge National Laboratory, Oak Ridge, Tennessee, 37831, USA*

<sup>4</sup>*Uppsala University, Department of Physics and Astronomy, Box 516, 75120, Uppsala, Sweden*

<sup>5</sup>*Swiss-Norwegian Beamlines, European Synchrotron Radiation Facility, 38043 Grenoble, France*

<sup>6</sup>*Siberian Federal University, 660041 Krasnoyarsk, Russia*

<sup>7</sup>*Kirensky Institute of Physics RAS, 660036 Krasnoyarsk, Russia*

<sup>8</sup>*Institute for Materials Research, Helmholtz-Zentrum Geesthacht, 21502 Geesthacht, Germany*

Chiral magnetism that manifests in the existence of skyrmions or chiral domain walls offers an alternative way for creating anisotropies in magnetic materials that might have large potential for application in future spintronic devices. Here we show experimental evidence for a new type of in-plane exchange bias effect present at room temperature that is created from a chiral 90° domain wall at the interface of a ferrimagnetic (DyCo)/ferromagnetic (NiFe) bilayer system. The chiral interfacial domain wall forms due to the orthogonal exchange coupling of NiFe and DyCo at the interface and the presence of Dzyaloshinskii-Moriya interaction in the DyCo layer. As a consequence of the preferred chirality of the interfacial domain wall, the sign of the exchange bias effect can be reversed by changing the perpendicular orientation of the DyCo magnetization. The chirality created tunable exchange bias in DyCo/NiFe is very robust against high in-plane magnetic fields ( $\mu_0 H \leq 6T$ ) and does not show any aging effects, therefore, it overcomes the limitations of conventional exchange bias systems.

## INTRODUCTION

Since the discovery of the exchange bias (EB) effect in 1950s by Meiklejohn and Bean when studying Co particles embedded in their native antiferromagnetic oxide [1] it has been intensively investigated due to its importance in magnetic spin valves and their applications in data storage technology [2, 3]. Despite its wide application, the EB effect is still not completely understood due to the technological limitations involved in directly observing and manipulating spin structures at an atomically thin magnetic interface [4, 5]. It is generally considered to form from an uncompensated spin configuration at the ferromagnetic (FM)/antiferromagnetic (AFM) interface with both frozen and rotatable spins [6–10]. Besides the classical system, EB related effects have also been observed in ferrimagnetic (FI) based materials with compensated interfaces [11–17]. Moreover, an atomic EB has been reported in a single ferrimagnetic DyCo<sub>4</sub> thin film where the magnetic surface region pins the magnetization of the bulk [18].

Recently, chiral ferrimagnetism was observed in amorphous GdCo films [19] due to the interfacial Dzyaloshinskii-Moriya interaction (DMI) effects [20, 21]. Besides, a new class of EB effect based on orthogonally exchange coupled systems has been proposed and observed [22–26]. Thereby, the DMI is suggested as a mechanism to drive the EB in G-Type antiferromagnetic perovskite interfaces [22] as well as in AFM/FM

IrMn<sub>3</sub>/Co(111) bilayer [23] or is accounted responsible for forming a tunable EB effect in dilute magnetic alloys [24]. A new form of magnetic anisotropy, originating from the tilted magnetization at the edges of magnetic structures due to the DMI, has been investigated in MgO/CoFeB/Pt [25] and Pt/Co/Ir [26]. In the latter case an out-of-plane EB-like effect was found when using an additional in-plane magnetic field. In a similar way a chirality-induced asymmetric domain nucleation in Pt/Co/AlO<sub>x</sub> with perpendicular magnetic anisotropy was observed when using in-plane magnetic fields [27]. The latter studies demonstrate effective paths for using DMI and DMI-like effects for creating and manipulating EB effects with a high potential for future applications. Moreover, the presence of DMI in magnetic thin film systems can lead to the creation of chiral domain walls (DW), that enable a surprisingly fast current-driven DW motion [28–35], while the velocity and the direction can be controlled by interfacial engineering [35–37].

Here, we report on a new approach to create a robust and tunable EB effect at room temperature that is based on a chiral interfacial domain wall ( $\sim 90^\circ$ ) present at the interface of orthogonally coupled layers of ferrimagnetic DyCo and ferromagnetic NiFe. Results from superconducting quantum interference device (SQUID), magneto-optical kerr effect (MOKE), and polarized neutron reflectivity (PNR) confirm the presence of an interfacial domain wall with a preferred chirality whose origin

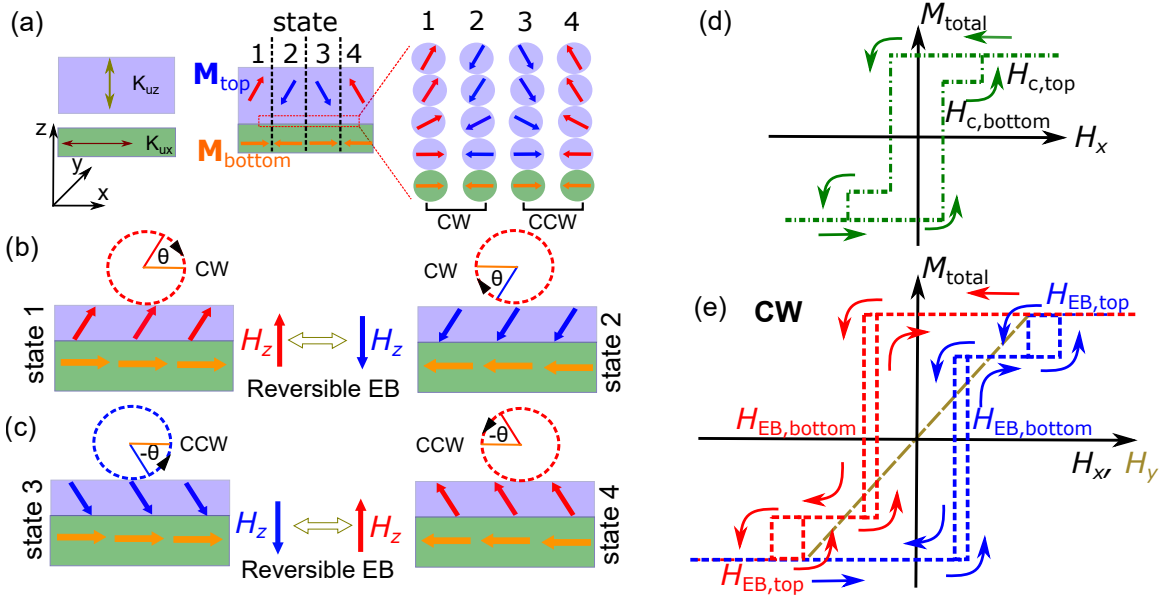


FIG. 1. Schematic picture of an exchange bias effect created from chiral interfacial domain wall. The figure illustrates magnetization profile in remanence and magnetization reversal along the x-axis for a magnetic bilayer system with an orthogonal exchange coupling: (a) For a bilayer with orthogonal UMA (represented by the anisotropy constants  $K_{ux}$  and  $K_{uz}$ ) and ferromagnetic exchange coupling at the interface, a two-step hysteresis loop results when the magnetic field is applied along the x-axis (d). In the presence of DMI at the interface, the four interfacial spin textures (marked as 1, 2, 3 and 4) become energetically unequal and a preferred (b) clockwise (CW) or (c) counter clockwise (CCW) spin rotation from top to bottom layer exists (represented by a positive or negative angle  $\theta$ ). (e) As shown for the CCW scenario, the DMI effect induces a dual EB effect for the switching of the top and the bottom layer, marked as  $H_{EB,top}$  and  $H_{EB,bottom}$ , resulting in a shifted in-plane hysteresis when the out of plane magnetization of the top layer is fixed. The sign of the in-plane EB effects can be switched by an out-of plane magnetic field  $H_z$  that changes the orientation of  $M_z$  of the top layer. (e) In the case of a favorable CCW spin rotation a negative (red) or positive (blue) shift of the  $M_x(H_x)$  hysteresis exists for a downward or upward magnetization  $M_z$  of the top layer, while no shift (brown) is expected for the  $M_y(H_y)$  hysteresis.

can be explained with the presence of the DMI effect in the DyCo layer.

### Concept of chirality created exchange bias

The magnetization profile in a bilayer system strongly depends on magnetic anisotropies present in the layers and the nature of the magnetic interactions occurring at the interface. In Fig. 1a, a bilayer system consisting of two planar films is considered exhibiting uniaxial magnetic anisotropies (UMA) whose easy axes (as marked as  $K_{ux}$  and  $K_{uz}$ ) are oriented perpendicular to each other. The exchange coupling at the interface results in a slightly tilted effective easy axis as illustrated for the top layer in Fig. 1(a). Such tilted magnetic configurations were experimentally observed e.g. in orthogonally exchange coupled [Co/Pd]/NiFe and CoPt/NiFe exchange spring systems [38, 39], or achieved by resputtering processes [40] or by using curved surfaces as substrates [41, 42]. The coupling between both layers will lead to four energetically equivalent interfacial spin textures, marked as 1, 2, 3, and 4, with their spins from top to bottom aligned as up-right, down-left, down-right and up-left. In the case

of a pinning of the magnetization component  $M_{top,z}$  of the top layer along one of the out-of-plane directions, a two-step hysteresis loop will be observed when a magnetic field is applied along the x-axis (Fig. 1d). Such a two step hysteresis loop as well as training effect of the exchange bias has been observed in the coupled ferromagnetic bilayer structures of CoCr/Ru/CoPtCrB. [43]

We propose a way to form a tunable exchange bias effect by lifting the degeneracy between the states with different chirality of the interfacial domain walls. The chirality refers here to the clockwise (CW) or counter clockwise (CCW) spin rotation from the top to the bottom layer (CW for states 1,2, Fig. 1b; CCW for states 3,4, Fig. 1c). Such chiral domain walls can originate from the bulk-like DMI [20, 21] or the DMI due to the break of the inversion symmetry at the interface. The DMI favors spins on neighboring sites to be aligned orthogonally, thus the interplay between DMI and exchange coupling between both layers at the interface will lead to non-collinear spin textures with a preferred chirality. Depending on the orientation of the perpendicular component of magnetization in the top layer,  $M_{top,z}$ , a unidirectional shift of the hysteresis loop occurs (Fig. 1e). Hence, the direction of the EB shift can be controlled

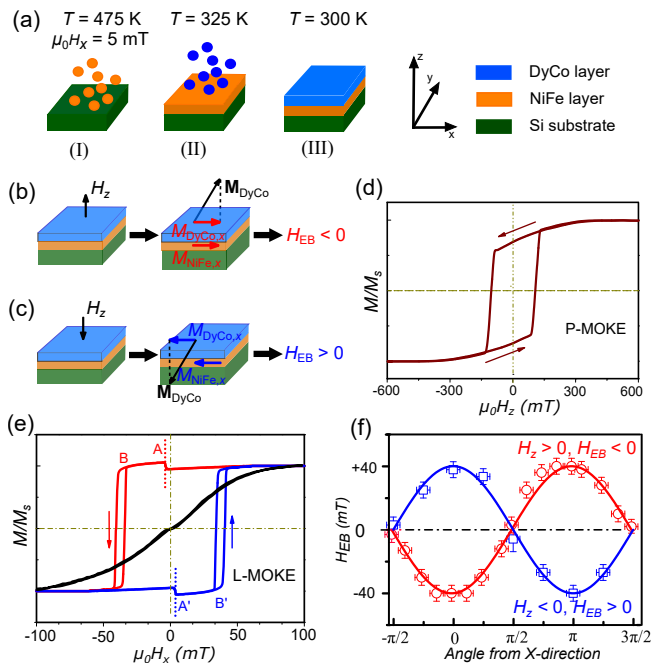


FIG. 2. Chirality created tunable EB effect in DyCo/NiFe. (a) Sample preparation: (I) The NiFe layer was deposited on a heated Si substrate ( $T=475$  K) at a magnetic in-plane field of  $5\text{mT}$ , (II) followed by the deposition of DyCo at  $T=325$  K, (III) while the magnetic characterization was performed at room temperature. (b), (c) The direction of the in-plane EB in DyCo/NiFe depends on the perpendicular component of magnetization of DyCo ((b)  $M_{DyCo,z} > 0$ :  $H_{EB} < 0$ , (c)  $M_{DyCo,z} < 0$ :  $H_{EB} > 0$ ). (d) Out-of-plane magnetic hysteresis loop ( $H \parallel z$ ), and (e) in-plane hysteresis loops for  $H$  perpendicular (black) and parallel to  $x$ -axis (red:  $M_{DyCo,z} > 0$  and blue:  $M_{DyCo,z} < 0$ ). The unidirectional shifts in the switching field for NiFe and DyCo are marked as A and B, or A' and B'. (f) Azimuthal angle dependence of the EB field after a pre-magnetization with  $\mu_0 H_z = -1$  T (blue curve) and  $\mu_0 H_z = +1$  T (red curve), respectively. The solid lines are  $\pm \cos\phi$  curves fitted to the data.

by setting  $M_{top,z}$  with a sufficiently strong out-of-plane magnetic field.

### Chirality created exchange bias effect in DyCo/NiFe

To realize a chiral interfacial domain wall in an orthogonally coupled system and create a tunable EB as it is shown in Fig. 1e, a bilayer consisting of ferromagnetic  $\text{Ni}_{80}\text{Fe}_{20}$  ( $\sim 130\text{nm}$ ) and ferrimagnetic  $\text{Dy}_{20}\text{Co}_{80}$  ( $\sim 70\text{nm}$ ) layer, denoted as DyCo/NiFe, was prepared on a Si wafer (Fig. 2a). In this system DyCo possesses a large perpendicular magnetic anisotropy while the soft magnetic NiFe layer shows an easy in-plane behavior. During the deposition of the individual layers, a small in-plane magnetic field of  $\mu_0 H = 5\text{mT}$  was applied to establish a uniaxial magnetic anisotropy (UMA) for the NiFe layer in the film plane. The easy axis of NiFe is denoted in

the following as the  $x$ -axis. At room temperature the ferrimagnetic DyCo layer is in the Co dominant phase ( $M_s^{Co} > M_s^{Dy}$ ) and the magnetic moments of Co and NiFe are ferromagnetically coupled at the interface.

The magnetization behavior of the DyCo/NiFe bilayer is investigated at room temperature using MOKE with the magnetic field applied perpendicular (P-MOKE:  $\mathbf{H} \parallel \pm z$ ) and parallel (L-MOKE:  $\mathbf{H} \parallel \pm x, \pm y$ ) to the sample plane. Fig. 2d shows the out-of-plane behavior with a coercive field of  $\mu_0 H_z \sim \pm 120\text{mT}$  revealing the switching of the magnetization of the DyCo layer. After the sample was magnetized along the surface normal with  $\mu_0 H_z = -1\text{T}$ , the bilayer is studied by L-MOKE. When the external magnetic field is applied along the  $x$ -axis direction, a positive shift of the hysteresis loop by  $\mu_0 H_{EB} = 39\text{mT}$  is observed confirming the occurrence of an in-plane EB effect in the bilayer (blue curve). If the in-plane magnetic field is applied, however, perpendicular to the  $x$ -axis, no exchange bias effect is found and the hysteresis loop exhibits a magnetic hard axis behavior (black curve). When the sample was magnetized with an opposite out-of-plane field ( $\mu_0 H_z = +1\text{T}$ ) the  $M_x(H_x)$  hysteresis gets shifted to negative field values (red curve), while the absolute value of the exchange bias field  $H_{EB}$  remains the same. This demonstrates that the direction of the EB effect can be switched by solely reversing the direction of the out-of-plane magnetization of DyCo.

For a switching of the EB direction, a magnetic field has to be applied along the out-of-plane direction that is sufficient to completely reverse  $M_z$  of the DyCo layer, i.e., the field has to be slightly larger than the coercive field of  $|\mu_0 H_c| = 120\text{mT}$ . Once established, the EB persists unaltered even after applying magnetic fields of more than  $\mu_0 H = 6\text{T}$  in the film plane. Fig. 2f shows the azimuthal angle dependence of the EB field taken after the sample was magnetized with  $\mu_0 H_z = \pm 1\text{T}$ . Within the error bar the azimuthal behavior of the EB can be well fitted with a  $\cos\phi$  function with  $\phi$  denoting the angle between the external field and the  $x$ -axis of the sample and thus following the behavior of classical EB systems.

Besides the prominent magnetization reversal at  $\mu_0 H_{EB} = 39\text{mT}$ , marked as B and B' in Fig. 2(e) for both pre-magnetized states, additional kinks are observed at low magnetic fields ( $\sim \pm 3\text{mT}$ ), marked as A and A'. The kinks corresponds to the switching of the NiFe layer, hence a dual exchange bias effect exists for the switching of the bilayer. Note that the signs of magneto-optical constants of NiFe and DyCo are opposite to each other, so that it wrongly appears that the NiFe layer switches antiparallel to the field. This misleading feature does not occur for SQUID technique. SQUID measurements were applied to gain complementary information of the magnetization behavior of the bilayer system, since MOKE is limited in penetration depth and is therefore mainly sensitive to the DyCo layer.

Fig. 3a shows the in-plane SQUID hysteresis curve for

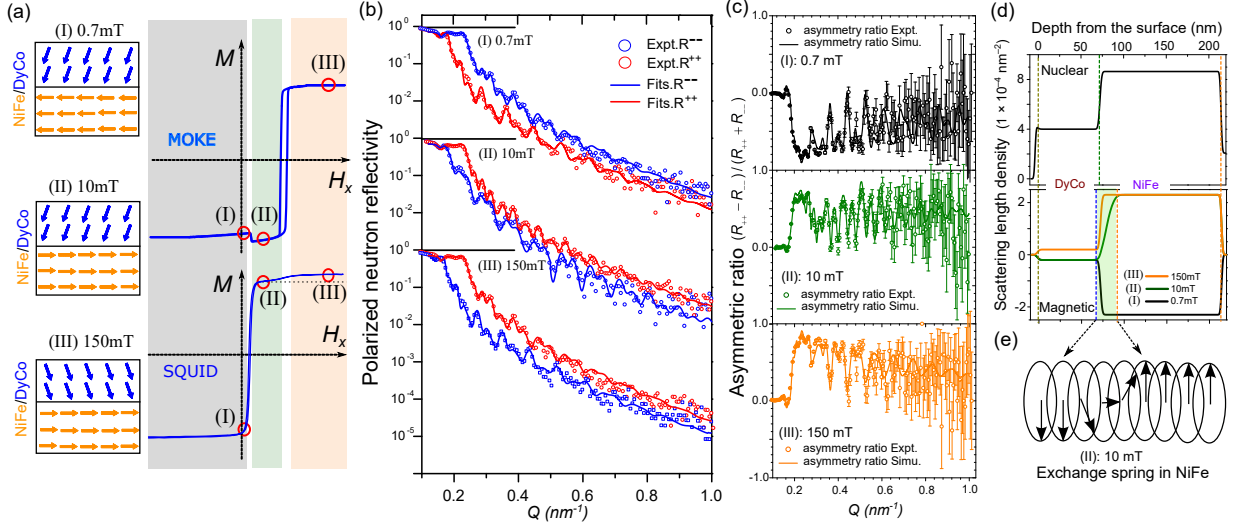


FIG. 3. Chiral interfacial domain wall. (a) Sketch of the three magnetic states marked as (I), (II), and (III) that are obtained from the MOKE and SQUID hysteresis loops. (b) Polarized Neutron Reflectivity (PNR) data (Expt.), and the results of the simulation (fits) taken at in-plane fields of  $\mu_0 H = 0.7, 10$  and  $150$  mT for spin up (red) and spin down neutrons (blue), representing the three states given in (a) obtained after the sample was premagnetized at a field of  $\mu_0 H_z = -1$  T in the out-of-plane direction. (c) Spin-asymmetry (SA) ratio  $SA = (R^{++} - R^{--}) / (R^{++} + R^{--})$  for the three spin states. (d) Nuclear and magnetic scattering length density (NSLD and MSLD) profiles of DyCo/NiFe layers obtained from the simulation. Magnetic states of (I), (II) and (III) are clearly observed, which are well separated by the two reversible kinks at  $\mu_0 H_{EB} = 3$  mT and  $39$  mT. For the state (II), the transition regime in the MSLD data (green area) indicates an exchange spring like spin texture (only the in-plane component) at the interface (e) for  $3 < \mu_0 H_x < 39$  mT.

pre-magnetization of  $\mu_0 H_z = -1$  T with its main signal slightly shifted with respect to zero magnetic field in absolute accordance with the position of the small kink A' present in the L-MOKE measurement. The SQUID signal is dominated by the magnetization of the NiFe layer which is much larger than the magnetization of the ferromagnetic DyCo layer, confirming that the kinks A' originate from the magnetic switching of the NiFe layer. However, a tiny kink reflecting the switching of the DyCo at  $\mu_0 H_x = 3$  mT is also observed in the SQUID measurements confirming the presence of the dual EB effect. From the results about the dual EB (Fig. 2 and 3) and the comparison with Fig. 1 we finally can conclude that for DyCo/NiFe a CW chirality is favored for the interfacial domain wall.

### Field dependent magnetic structures

To understand the underlying spin structure providing the EB effect in more detail, we employed polarized neutron reflectivity (PNR) measurements which enables to probe the nuclear and magnetization depth profiles for the different magnetic states [44–46]. According to the results of the L-MOKE and SQUID measurements, the DyCo layer has a slightly tilted magnetic configuration in the  $xz$ -plane while the magnetic moments of the NiFe layer are aligned along the  $x$ -axis. Con-

sidering the different in-plane switching fields for DyCo and NiFe, there are three principle field-dependent magnetic states in the bilayer, marked as (I), (II) and (III) in Fig. 3a. For these states, the details of the nuclear profile and the magnetization vector configuration were revealed from the analysis of the non-spin flip reflectivities  $R^{++}$  (spin up neutrons) and  $R^{--}$  (spin down neutrons) and the corresponding spin-asymmetry (SA) ratios  $SA = (R^{++} - R^{--}) / (R^{++} + R^{--})$  shown in Fig. 3b and 3c, respectively. The corresponding profiles of the scattering length density (both nuclear and magnetic) are shown in Fig. 3d. The non-sharp transitions of the nuclear scattering length density at the surface, DyCo/NiFe and NiFe/Si interface are due to the roughnesses which were determined to be  $2.0, 2.2,$  and  $1.6$  nm, respectively, from the fittings.

First, a small in-plane magnetic field of  $+0.7$  mT was applied along the  $x$ -axis after the initial out-of-plane magnetic field of  $-1$  Tesla was switched off (state (I)). A simultaneous fit to the experimental reflectivity with opposite polarization states ( $R^{++}$  and  $R^{--}$ ) shows that the in-plane component of magnetization of both DyCo and NiFe layers are magnetized along the same in-plane direction, antiparallel to the direction of the external field in agreement with SQUID and MOKE measurements (Fig. 3a). The assumption of a constant, uniform in-plane magnetization inside both layers leads to a very good agreement between the experimental and the-

oretical curves. The result at quasi-zero magnetic field demonstrates that the system has a preference for a certain in-plane orientation of magnetization after it is pre-magnetized beforehand along one of the out-of-plane directions.

At  $\mu_0 H_x = 10mT$  (state (II)), clear changes in the polarized reflectivity curves are observed. The fit to the experimental data shows that the in-plane magnetization direction of the NiFe has switched along the direction of the field while the in-plane component of DyCo magnetization remains still orientated in the previous, opposite direction. For this oppositely aligned magnetic layer configuration, PNR reveals the existence of a  $\sim 20nm$  thick interfacial region (much larger than the interface roughness of  $2.2 nm$ ) where the in-plane magnetization gradually changes from opposite to field magnetized DyCo to field aligned magnetization of NiFe. It indicates the formation of an interfacial layer where the magnetic moments are perpendicularly oriented to the applied magnetic field as it is the case for non-collinear spin structures like e.g. exchange spring structures (Fig. 3e), similar to what was observed in a CoPt/Permalloy/Ta/Permalloy heterostructure [46]. After increasing the external magnetic field above  $H_{EB}$  of the DyCo layer ( $\mu_0 H_x = 150mT$ , state (III)), the PNR results reveal that the in-plane components of the magnetization of both layers are field aligned. The magnetization profile around the interface of both layers follows again the chemical profile.

Summarizing the complementary results from MOKE, SQUID, and PNR techniques, the scenario for the presence of a chiral interfacial domain wall with CW chirality as depicted in Fig. 1c has been confirmed. During the initial application of an external magnetic field along the out-of-plane direction ( $\mu_0 H_z \geq 120mT$ ) the magnetization of DyCo and NiFe layers follows the applied field and the z-component of DyCo switches along the field direction. After the magnetic field is switched off, the NiFe moments follow their in-plane UMA, turning their moments along the negative or positive x-axis depending on the orientation of  $M_{DyCo,z}$ . The PNR data, with the absence of the off-specular scattering, clearly demonstrate that such a single domain state is created. The resulting DyCo moments, that are exchange coupled at the interface to the NiFe layer, partly follow the NiFe moments into the in-plane direction leading to a tilted configuration. By applying an in-plane magnetic field along the opposite direction of the orientation of the NiFe and DyCo moments, first the NiFe moments start to reverse, slightly exchange-biased, until the in-plane orientation of NiFe and DyCo are antiparallel aligned (state (I)  $\rightarrow$  state (II) in Fig. 3a). At this stage the magnetic configuration at the interface leads to an interfacial regime that can be pictured as an exchange spring structure. When the magnetic field exceeds the larger EB field of  $39mT$ , the in-plane magnetization of the DyCo layer finally also reverses and aligns along the field direction as depicted in

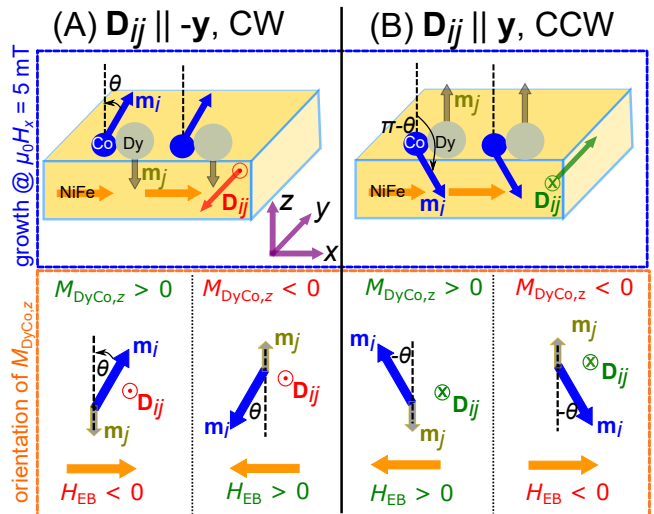


FIG. 4. Microscopic origin of the chirality created tunable EB effect. Upper Figure: During the growth process the application of an in-plane field  $\mu_0 H_x = 5mT$  provides a uniaxial anisotropy and a field aligned single domain state in NiFe. With the ferromagnetic coupling between the Co and the NiFe atoms at the interface, two possible magnetization configuration may form when the DyCo layer is deposited on NiFe which are energetically degenerate in the case of vanishing DMI. State (A) (or (B)) is favored in the case of negative (positive) DMI constant  $D_{ij}$  in DyCo along the y-direction (i:Co, j:Dy) corresponding to a CW (CCW) chirality of the interfacial domain wall between NiFe and Co. Lower Figure: The sign of the perpendicular component of magnetization of the DyCo layer  $M_{DyCo,z}$  (Co moments  $m_i$ ) dictates the sign field  $H_{EB}$ . For  $D_{ij} > 0$  or  $D_{ij} < 0$  (CW or CCW chirality of interfacial DW),  $M_{DyCo,z}$  and  $H_{EB}$  have opposite signs.

state (III) of Fig. 3a, resolving the spring structure at the interface.

### Origin of the chiral domain wall

During the growth of the DyCo alloy onto the NiFe layer, the latter is in a single domain state with the moments pointing along the x-axis due to the applied field of  $\mu_0 H_x = 5mT$ . Because of the ferromagnetic coupling between Co and NiFe moments, the Co moments get slightly tilted away from the perpendicular easy axis along the x-direction with the option to point upward (state A) or downward (state B), respectively (upper sketch in Fig. 4). Since the presence of the EB effect revealed that a CW chirality of the interfacial domain wall is favored the Co moments tilt upward. Note that due to the cone spin structure of Dy [60] and its weak coupling to the NiFe layer, the averaged in-plane magnetic component of Dy is relatively small and, for the sake of clarity, neglected in the following discussion as depicted in Fig. 4. Hence, the magnetic moments of Co and Dy atoms at neighboring atomic sites i and j can be

written as  $\mathbf{m}_i = a_1\vec{x} + c_1\vec{z}$  and  $\mathbf{m}_j = c_2\vec{z}$ , respectively, with  $a_1$ ,  $c_1$  and  $c_2$  representing the Co and Dy magnetic components along  $+x$  and  $+z$  axes.

In order to understand the origin of the EB effect a possible DMI effect between Co and Dy moments is considered whose contribution to the free energy is generally written as  $E_{DM} \propto D_{ij}(s_i \times s_j)$  where  $D_{ij}$  is the DM vector and  $s_i$  and  $s_j$  are the respective spins. [20, 21]. In consideration of a homogeneous, non-zero DM vector  $D_{ij}$  along the  $+y$  ( $D_{ij} > 0$ ) or the  $-y$  ( $D_{ij} < 0$ ) axis, the contribution of the DMI effect to the free energy is  $a_1c_2 \cdot D_{ij}^y$ , lifting the degeneracy between state (A) and (B) shown in Fig. 4. Therefore a preferred tilting of the magnetization with the angle of  $\theta$  or  $-\theta$  with respect to the film normal exists and the sign of the angle depends on whether  $D_{ij}^y$  points along the  $-y$  or  $+y$  axis. All other projections of the DM vector cannot give any contribution to the preferred chirality.

Due to the ferromagnetic exchange coupling between the Co and NiFe moments, the chiral effect in DyCo is transferred to the moments ( $m_{NiFe}$  and  $m_{Co}$ ) at the interface and therefore a preferred chirality for the interfacial domain wall exists as depicted in the lower panel of Fig. 4. Without the presence of a macroscopic DMI during the growth procedure, the energies of clockwise (CW) and counter clockwise (CCW) chiral spin structure at the interface are equal and no EB effect would be observed. For a CW chirality as favored for DyCo/NiFe the DM vector points along  $-y$ -direction.

In order to estimate the strength of the DMI, we take into account that a reverse field of  $\mu_0H_x = 39$  mT is required to generate the DMI-unfavored orientation between the Co and Dy spins (state III in Fig. 3(a) and state (B) in Fig. 4). Hence, at this magnetic field the Zeeman energy overcompensates the DMI energy in the DyCo layer:  $E = \mu_0H_x\Delta M_S^{DyCo}$ . According to the SQUID data shown in Fig. 3(a) the in-plane component in DyCo changes by  $\Delta M_S^{DyCo} \approx 65kA m^{-1}$ . Consequently,  $E \approx 2.5kJ m^{-3}$  results for the bulk DMI energy density between Dy and Co moments. The remaining question is, if the DMI is inherently present in the whole DyCo layer [67] or only exists in the DyCo atomic layers next to the interface [19] triggered by the adjacent NiFe layer. A bulk DMI in GdFeCo amorphous ferrimagnets has been reported, attributed to an asymmetric distribution of the elemental content[67]. Even though no evidence can be provided here for such an asymmetric distribution of the Dy and Co elements, the finding of an asymmetric magnetization from the surface to the bulk in a thin film of DyCo<sub>4</sub>[18] suggests the existence of a bulk-like DMI in the DyCo system. Then the effective DMI constant can be estimated to be  $D_{eff} = E \times t = 0.18mJ m^{-2}$  with  $t$  the thickness of DyCo layer of  $70 nm$ . The value of  $0.18 mJ m^{-2}$  follows the value of GdFeCo when extrapolated to  $70 nm$  [67]. This value is one order of magnitude smaller than the pro-

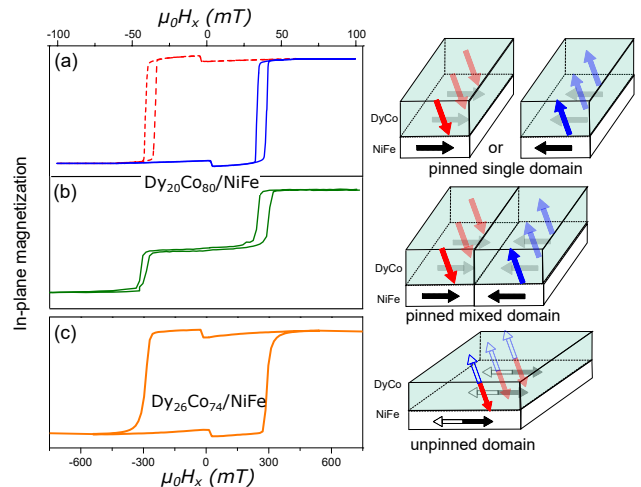


FIG. 5. Connection between EB effect and domain stability. Three scenarios are depicted with the experimentally measured hysteresis loops (left) and the corresponding domain state configurations (right). (a) and (b) demonstrate the results for the system Dy<sub>20</sub>Co<sub>80</sub>/NiFe bilayer, (a) for the single domain state with  $M_{z,DyCo} < 0$  (red) and  $M_{z,DyCo} > 0$  (blue), respectively, and (b) for the multi-domain state where up and down domains exist simultaneously. (c) shows the scenario for a switching of  $M_{DyCo,z}$  during the  $H_x$ -field application measured for a Dy<sub>26</sub>Co<sub>74</sub>/NiFe bilayer.

totypical Pt/Co interface (of the order of  $\sim mJ m^{-2}$ )[68], in which Neel domain walls or skyrmions are stabilized [47, 48] and the DMI energy is contributed from the width of the domain wall region. Even though the  $D_{eff}$  is much weaker here, the value is significant since the whole interfacial area contributes to the DMI energy and thus to the observed chirality effect. In order to distinguish between bulk and interface DMI effect, one has to determine the DMI strength as a function of DyCo thickness. Such studies are foreseen in the future.

The DMI induced chiral interfacial domain wall is not the only mandatory requirement for generating the EB effect in DyCo/NiFe. As illustrated in Fig. 5, it also requires the stability of the out-of-plane magnetic component, in particular, it may not reverse under the application of an in-plane magnetic field. As shown in Fig. 5a, a dual in-plane exchange bias effect exists when a single domain state was formed in the DyCo layer. In contrast, in the case of a multi-domain state with up and down domains in the DyCo layer, which can e.g. be generated by the application of a reversed out-of-plane magnetic field equal to the coercive field, a double shifted in-plane hysteresis loop with two steps is observed (Fig. 5b). The relative amount between both out-of-plane domains remains unchanged even after the application of a high magnetic in-plane field. Without this domain stability in the ferromagnetic layer the described chirality created EB effect cannot be established on a laterally macroscopic scale. Such a case without domain stability is shown in Fig. 5c

depicting the in-plane hysteresis of a  $\text{Dy}_{26}\text{Co}_{74}/\text{NiFe}$  bilayer system. Here the out-of-plane magnetization of the  $\text{Dy}_{26}\text{Co}_{74}$  layer, with a different compensation temperature and magnetic anisotropy from  $\text{Dy}_{20}\text{Co}_{80}$  [18, 59–62], completely switches during the hysteresis resulting in an axial symmetric loop without the presence of the EB effect. However, the fingerprint of the chiral DW at the  $\text{DyCo}/\text{NiFe}$  interface, i.e., the occurrence of two steps in the hysteresis, still persists even for this alloy composition. The reason for the domain instability is the higher Dy concentration in the  $\text{DyCo}$  layer which leads to a reduced perpendicular magnetic anisotropy at room temperature, so that the  $\text{DyCo}$  magnetization gets susceptible and can be switched even by the application of low in-plane magnetic fields.

### Conclusion

In conclusion, we report on a tunable in-plane EB effect we observed at room temperature in  $\text{DyCo}/\text{NiFe}$  bilayer system that is stable on a macroscopic scale up to high in-plane magnetic fields ( $\mu_0 H \leq 6$  T). The direction of the EB effects can be switched and controlled by the direction of a moderate magnetic field applied along the out-of-plane direction beforehand. The results from complementary MOKE, SQUID, and PNR measurements leads to the conclusion that the EB effect originates from the chiral spin texture of the interfacial domain wall. The creation of the chiral interfacial domain wall is a consequence of the interplay between DMI in  $\text{DyCo}$  and ferromagnetic exchange coupling between both  $\text{NiFe}$  and  $\text{DyCo}$  layers whose uniaxial anisotropies are orthogonally oriented to each other. Realizations of isothermal EB switching have been reported earlier by means of local electric fields [49–56] and magnetic fields [57, 58]. Here the chirality created tunable EB effect may introduce a new approach to overcome the limitations of conventional EB systems. The use of an easy and fast production path via standard sputtering techniques to create a chiral domain wall for establishing a sizeable exchange bias effect makes this film system very attractive for the application in future spintronic devices. Particularly, the flexibility in controlling exchange bias at room temperature could be exploited in future spintronic devices and new concepts where e.g. the storage density can be increased allowing more as the standard dual logical states, with thermomagnetic data erasing and writing[65, 66]. Besides, the extreme stability of the exchange bias effect even at very high magnetic fields without any observable training effect is a very important feature for the fabrication of long-living spintronic devices. Finally, the creation of chiral interfacial domain walls in thin film systems provides a possible way to control the out-of-plane magnetization by the application of an in-plane magnetic field. However, compared to the frequently discussed chi-

ral spin textures of skyrmions, further investigations on the dynamics and transport properties of such chiral interfacial domain walls are required to determine their full potential for technological applications.

K.C. benefited from the support of the German funding agency DFG (Project No. 615811). A.P.-K. gratefully acknowledge support from DFG via SFB925.

### Sample Preparation and characterization

The  $\text{Dy}_{20}\text{Co}_{80}/\text{Ni}_{80}\text{Fe}_{20}$  film was fabricated by thermal evaporation in vacuum of  $3 \times 10^{-10} \text{ Torr}$  by successively sputtering the  $\text{NiFe}$  and  $\text{DyCo}$  layers from independent evaporators ( $\text{NiFe}$ ,  $\text{Dy}$ ,  $\text{Co}$ ) with a ring cathode onto  $\text{Si}(110)$  substrates.  $\text{NiFe}$  was deposited on  $\text{Si}(110)$  at  $T=475\text{K}$  at  $\mu_0 H = 5\text{mT}$  applied along the x-axis, and  $\text{DyCo}$  was co-deposited at  $T=325\text{K}$  and  $\text{DyCo}/\text{NiFe}$  bilayer was finally cooled to room temperature. The deposition rates were identical at  $0.5\text{nm/s}$ . In good agreement with the PNR fittings, the thicknesses of the  $\text{NiFe}$  and  $\text{DyCo}$  determined by x-ray reflectivity measurements are  $139 \pm 5\text{nm}$  and  $70 \pm 2\text{nm}$ , respectively. Since for  $\text{DyCo}$ , the room temperature compensation composition is between  $\text{Dy}_{21}\text{Co}_{79}$  and  $\text{Dy}_{24}\text{Co}_{76}$ [18, 60–62], the net magnetization in the ferrimagnetic  $\text{Dy}_{20}\text{Co}_{80}$  is equal to  $M = M^{\text{Co}} - M^{\text{Dy}}$ . The in-plane magnetic field applied during the sample preparation that imprints the uniaxial anisotropy is required for the EB effect. In similar samples prepared without field during the growth of the films, no preferred in-plane tilting direction is established resulting in the absence of a macroscopically observable EB effect.

Polarized Neutron Reflectivity (PNR) was applied to investigate the magnetic depth profile of the sample and, in particular, to gain depth dependent information about the changes in the magnetic structure for the different magnetic states. The PNR measurements were performed at the Super-ADAM reflectometer at the ILL in collaboration with university of Uppsala and on the Magnetism Reflectometer (beamline BL-4A)[63] at the Spallation Neutron Source of Oak Ridge National Laboratory. The PNR spectra were taken for several external magnetic fields applied along the x-axis of the sample using polarization analysis, in particular to extract non-spin-flip intensities that are sensitive to the magnetic moments along the applied magnetic guide field, i.e.  $R^{++}$  and  $R^{--}$  for the magnetic moments aligned parallel and anti-parallel to the applied in-plane field, respectively. It should be noted that PNR is only sensitive to magnetic moments perpendicular to the momentum transfer vector  $Q$  of the measurement, i.e. only the in-plane magnetization is detected. The measured reflectivity curves were analyzed using the method of Parratt[64]. Prior the PNR measurements the sample was pre-magnetized in a magnetic field of  $\mu_0 H = -1\text{T}$  in the out-of-plane direc-

tion to establish the EB effect as observed in the MOKE measurements.

The thickness and nuclear scattering length densities (NSLD) are  $70 \pm 2$  (nm) and  $3.95 \times 10^{-4}$  (nm<sup>-2</sup>) for the layer of DyCo and  $139 \pm 5$  (nm) and  $8.6 \times 10^{-4}$  (nm<sup>-2</sup>) for the layer of NiFe, respectively. The magnetic moments can be calculated from the magnetic scattering length densities (MSLD) of the fits. A MSLD of  $2.05 \pm 0.05 \times 10^{-4}$  (nm<sup>-2</sup>) for the NiFe layer corresponds to a magnetic moment of  $0.96 \mu_B$  per NiFe formula unit while DyCo due to its ferrimagnetic coupling between both sites shows with a MSLD of  $0.45 \pm 0.05 \times 10^{-4}$  (nm<sup>-2</sup>) only a much lower magnetization of  $0.2 \mu_B$  per DyCo formula unit.

---

\* kaichen.hzg@gmail.com

- [1] W. H. Meiklejohn and C. P. Bean, New magnetic anisotropy, *Phys. Rev.* **102**, 1413 (1956).
- [2] S. Parkin, J. Xin, C. Kaiser, A. Panchula, K. Roche, and M. Samant, Magnetically engineered spintronic sensors and memory, *Proc. IEEE* **91**, 661 (2003).
- [3] C. Chappert, A. Fert, and F. N. V. Dau, The emergence of spin electronics in data storage, *Nat. Mater.* **6**, 813-823 (2007).
- [4] J. Nogues and I. K. Schuller, Exchange bias, *J. Magn. Magn. Mater.* **192**, 203 (1999).
- [5] M. Kiwi, Exchange bias theory, *J. Magn. Magn. Mater.* **234**, 584 (2001).
- [6] H. Ohldag, F. Scholl, A. and Nolting, E. Arenholz, S. Maat, A. T. Young, M. Carey, and J. Stohr, Correlation between exchange bias and pinned interfacial spins, *Phys. Rev. Lett.* **91**, 017203 (2003).
- [7] F. Radu, S. K. Mishra, I. Zizak, A. I. Erko, H. A. Dürr, W. Eberhardt, G. Nowak, S. Buschhorn, H. Zabel, K. Zhernenkov, M. Wolff, D. Schmitz, E. Schierle, E. Dudzik, and R. Feyerherm, Origin of the reduced exchange bias in an epitaxial FeNi(111)/CoO(111) bilayer, *Phys. Rev. B* **79**, 184425 (2009).
- [8] S. K. Mishra, F. Radu, S. Valencia, D. Schmitz, E. Schierle, H. A. Dürr, and W. Eberhardt, Dual behavior of antiferromagnetic uncompensated spins in NiFe/IrMn exchange biased bilayers, *Phys. Rev. B* **81**, 212404 (2010).
- [9] J. Wu, J. S. Park, W. Kim, E. Arenholz, M. Liberati, A. Scholl, Y. Z. Wu, C. Hwang, and Z. Q. Qiu, Direct measurement of rotatable and frozen CoO spins in exchange bias system of CoO/Fe/Ag(001), *Phys. Rev. Lett.* **104**, 217204 (2010).
- [10] R. Morales, A. C. Basaran, J. E. Villegas, D. Navas, N. Soriano, B. Mora, C. Redondo, X. Battle, and I. K. Schuller, Exchange-Bias Phenomenon: The role of the ferromagnetic spin structure, *Phys. Rev. Lett.* **114**, 097202 (2015).
- [11] F. Hellman, R. B. van Dover, and E. M. Gyorgy, Unexpected unidirectional anisotropy in amorphous Tb-Fe/Ni-Fe-Mo bilayer films, *Appl. Phys. Lett.* **50**, 296 (1987).
- [12] W. C. Cain and M. H. Kryder, Investigation of the exchange mechanism in NiFe-TbCo bilayers, *J. Appl. Phys.* **67**, 5722 (1990).
- [13] F. Radu, R. Abrudan, I. Radu, D. Schmitz, and H. Zabel, Perpendicular exchange bias in ferrimagnetic spin valves, *Nat. Comm.* **3**, 715 (2012).
- [14] A. K. Nayak, M. Nicklas, S. Chadov, P. Khuntia, C. Shekhar, A. Kalache, M. Baenitz, Y. Skourski, V. K. Guduru, A. Puri, U. Zeitler, J. M. D. Coey, and C. Felser, Design of compensated ferrimagnetic Heusler alloys for giant tunable exchange bias, *Nat. Mater.* **14**, 679-684 (2015).
- [15] S.M. Watson, Thomas Hauet, J. A. Borchers, S. Mangin, Eric E. Fullerton, Interfacial magnetic domain wall formation in perpendicular-anisotropy, exchange-spring films, *Appl. Phys. Lett.* **92**, 202507 (2008).
- [16] C. Schubert, B. Hebler, H. Schletter, A. Liebig, M. Daniel, R. Abrudan, F. Radu, and M. Albrecht, Interfacial exchange coupling in Fe-Tb/[Co/Pt] heterostructures, *Phys. Rev. B* **87**, 054415 (2013).
- [17] B. Hebler, P. Reinhardt, G. L. Katona, O. Hellwig, and M. Albrecht, Double exchange bias in ferrimagnetic heterostructures, *Phys. Rev. B* **95**, 104410 (2017).
- [18] K. Chen, D. Lott, F. Radu, F. Choueikani, E. Otero, and P. Ohresser, Observation of an atomic exchange bias effect in DyCo4 film, *Sci. Rep.* **5**, 18377 (2015).
- [19] R. Streubel, C.-H. Lambert, N. Kent, P. Ercius, A. T. N'Diaye, C. Ophus, S. Salahuddin and P. Fischer, Experimental evidence of chiral ferrimagnetism in amorphous GdCo films, *Adv. Mat.* **30**, 1800199 (2018).
- [20] I. E. Dzyaloshinskii, Thermodynamical theory of 'weak' ferromagnetism in antiferromagnetic substances, *Sov. Phys. JETP* **5**, 1259 (1957).
- [21] T. Moriya, Anisotropic superexchange interaction and weak ferromagnetism, *Phys. Rev.* **120**, 91 (1960).
- [22] S. Dong, K. Yamauchi, S. Yunoki, R. Yu, S. Liang, A. Moreo, J.-M. Liu, S. Picozzi, and E. Dagotto, Exchange bias driven by the Dzyaloshinskii-Moriya interaction and ferroelectric polarization at G-type antiferromagnetic perovskite interfaces, *Phys. Rev. Lett.* **103**, 127201 (2009).
- [23] R. Yanes, J. Jackson, L. Udvardi, L. Szunyogh, and U. Nowak, Exchange bias driven by Dzyaloshinskii-Moriya interactions, *Phys. Rev. Lett.* **111**, 217202 (2013).
- [24] R. M. Matthias Hudl and P. Nordblad, Tunable exchange bias in dilute magnetic alloys-chiral spin glasses, *Sci. Rep.* **6**, 19964 (2016).
- [25] M. Cubukcu, J. Sampaio, K. Bouzehouane, D. Apalkov, A. V. Khvalkovskiy, V. Cros, and N. Reyren, Dzyaloshinskii-Moriya anisotropy in nanomagnets with in-plane magnetization, *Phys. Rev. B* **93**, 020401 (2016).
- [26] D.-S. Han, N.-H. Kim, J.-S. Kim, Y. Yin, J.-W. Koo, J. Cho, S. Lee, M. Klui, H. J. M. Swagten, B. Koopmans, and C.-Y. You, Asymmetric hysteresis for probing Dzyaloshinskii-Moriya interaction, *Nano Lett.* **16**, 4438 (2016).
- [27] S. Pizzini, J. Vogel, S. Rohart, L. D. Buda-Prejbeanu, E. Jue, O. Boulle, I. M. Miron, C. K. Safeer, S. Auffret, G. Gaudin, and A. Thiaville, Chirality-induced asymmetric magnetic nucleation in Pt/Co/AlO<sub>x</sub> ultrathin microstructures, *Phys. Rev. Lett.* **113**, 047203 (2014).
- [28] M. Heide, G. Bihlmayer, and S. Blügel, Dzyaloshinskii-Moriya interaction accounting for the orientation of magnetic domains in ultrathin films: Fe/W(110), *Phys. Rev. B* **78**, 140403 (2008).
- [29] T. A. Moore, I. M. Miron, G. Gaudin, G. Serret, S. Auffret, B. Rodmacq, A. Schuhl, S. Pizzini, J. Vogel, and M.

- Bonfim, High domain wall velocities induced by current in ultrathin Pt/Co/AlO<sub>x</sub> wires with perpendicular magnetic anisotropy, *Appl. Phys. Lett.* **93**, 262504 (2008).
- [30] A. Thiaville, S. Rohart, E. Jue, V. Cros, and A. Fert, Dynamics of Dzyaloshinskii domain walls in ultrathin magnetic films, *Europhys. Lett.* **100**, 57002 (2012).
- [31] G. Chen, J. Zhu, A. Quesada, J. Li, A. T. N'Diaye, Y. Huo, T. P. Ma, Y. Chen, H. Y. Kwon, C. Won, Z. Q. Qiu, A. K. Schmid, and Y. Z. Wu, Novel chiral magnetic domain wall structure in Fe/Ni/Cu(001) Films, *Phys. Rev. Lett.* **110**, 177204 (2013).
- [32] S. Emori, U. Bauer, S. Ahn, E. Martinez, and G. S. D. Beach, Current-driven dynamics of chiral ferromagnetic domain walls, *Nat. Mater.* **12**, 611-616 (2013).
- [33] O. Boulle, S. Rohart, L. D. Buda-Prejbeanu, E. Jue, I. M. Miron, S. Pizzini, J. Vogel, G. Gaudin, and A. Thiaville, Domain wall tilting in the presence of the Dzyaloshinskii-Moriya interaction in out-of-plane magnetized magnetic nanotracks, *Phys. Rev. Lett.* **111**, 217203 (2013).
- [34] A. Brataas, Spintronics: Chiral domain walls move faster, *Nat. Nanotechnol.* **8**, 485-486 (2013).
- [35] J. Torrejon, J. Kim, J. Sinha, S. Mitani, M. Hayashi, M. Yamanouchi, and H. Ohno, Interface control of the magnetic chirality in CoFeB/MgO heterostructures with heavy-metal underlayers, *Nat. Comm.* **5**, 4655 (2014).
- [36] K. Ryu, L. Thomas, S. Yang, and S. Parkin, Chiral spin torque at magnetic domain walls, *Nat. Nanotechnol.* **8**, 527-533 (2013).
- [37] G. Chen, T. Ma, A. T. N'Diaye, H. Kwon, C. Won, Y. Wu, and A. K. Schmid, Tailoring the chirality of magnetic domain walls by interface engineering, *Nat. Comm.* **4**, 2671 (2013).
- [38] T. N. A. Nguyen, Y. Fang, V. Fallahi, N. Benatmane, S. M. Mohseni, R. K. Dumas, and J. Akerman, [Co/Pd]-NiFe exchange springs with tunable magnetization tilt angle, *Appl. Phys. Lett.* **98**, 172502 (2011).
- [39] P. Saravanan, J.-H. Hsu, C. L. Tsai, C. Y. Tsai, Y. H. Lin, C. Y. Kuo, J.-C. Wu, and C.-M. Lee, Interplay between out-of-plane anisotropic L11-type CoPt and in-plane anisotropic NiFe layers in CoPt/NiFe exchange springs, *J. Appl. Phys.* **115**, 243905 (2014).
- [40] A. Lisfi, J. C. Lodder, H. Wormeester, B. Poelsema, Reorientation of magnetic anisotropy in obliquely sputtered metallic thin films, *Phys. Rev. B.* **66**, 174420 (2002).
- [41] M. Albrecht, G. Hu, I. L. Guhr, T. C. Ulbrich, J. Boneberg, P. Leiderer, and G. Schatz, Magnetic multilayers on nanospheres, *Nat. Mater.* **4**, 203-206 (2005).
- [42] L. You, O. Lee, D. Bhowmik, D. Labanowski, J. Hong, J. Bokor, and S. Salahuddin, Switching of perpendicularly polarized nanomagnets with spin orbit torque without an external magnetic field by engineering a tilted anisotropy, *Proc. Natl. Acad. Sci.* **112**, 10310 (2015).
- [43] Ch. Binek, S. Polisetty, Xi He, and A. Berger, Exchange bias training effect in coupled all ferromagnetic bilayer structures, *Phys. Rev. Lett.* **96**, 067201 (2006).
- [44] C. Majkrzak, Polarized neutron reflectometry, *Physica B: Condens. Matt.* **173**, 75-88 (1991).
- [45] S. J. Blundell, M. Gester, J. A. C. Bland, H. J. Lauter, V. V. Pasyuk, and A. V. Petrenko, Asymmetric magnetization reversal in exchange-biased hysteresis loops, *Phys. Rev. Lett.* **84**, 3986 (2000).
- [46] Y. Wang, X. He, T. Mukherjee, M. R. Fitzsimmons, S. Sahoo, and Ch. Binek, Magnetometry and transport data complement polarized neutron reflectometry in magnetic depth profiling, *J. Appl. Phys.*, **110**, 103914 (2011).
- [47] C. Moreau-Lucaire, C. Moutafis, N. Reyren, J. Sampaio, C. A. F. Vaz, N. Van Horne, et al, Additive interfacial chiral interaction in multilayers for stabilization of small individual skyrmions at room temperature, *Nat Nanotechnol.* **11**, 444-448 (2016).
- [48] F. Hellman, A. Hoffmann, Y. Tserkovnyak, G. S. D. Beach, E. E. Fullerton, and C. Leighton, et al., Interface-induced phenomena in magnetism, *Rev. Mod. Phys.* **89**, 025006 (2017).
- [49] H. Ohno, D. Chiba, F. Matsukura, T. Omiya, E. Abe, T. Dietl, Y. Ohno, and K. Ohtani, Electric-field control of ferromagnetism, *Nature* **408**, 944-946 (2000).
- [50] P. Borisov, A. Hochstrat, X. Chen, W. Kleemann, and C. Binek, Magnetoelectric switching of exchange bias, *Phys. Rev. Lett.* **94**, 117203 (2005).
- [51] X. He, Y. Wang, N. Wu, A. N. Caruso, E. Vescovo, K. D. Belashchenko, P. A. Dowben, and C. Binek, Robust isothermal electric control of exchange bias at room temperature, *Nat. Mater.* **9**, 579-585 (2010).
- [52] W. G. Wang, M. Li, S. Hageman, and C. L. Chien, Electric-field-assisted switching in magnetic tunnel junctions, *Nat. Mater.* **11**, 64-68 (2012).
- [53] S. M. Wu, S. A. Cybart, D. Yi, J. M. Parker, R. Ramesh, and R. C. Dynes, Full electric control of exchange bias, *Phys. Rev. Lett.* **110**, 067202 (2013).
- [54] F. A. Cuellar, Y. H. Liu, J. Salafranca, N. Nemes, E. Iborra, G. S. Santolino, M. Varela, M. G. Hernandez, J. W. Freeland, M. Zhernenkov, M. R. Fitzsimmons, S. Okamoto, S. J. Pennycook, M. Bibes, A. Barthelmy, S. G. E. te Velthuis, Z. Sefrioui, C. Leon, and J. Santamaria, Reversible electric-field control of magnetization at oxide interfaces, *Nat. Comm.* **5**, 4215 (2014).
- [55] F. Matsukura, Y. Tokura, and H. Ohno, Control of magnetism by electric fields, *Nat. Nanotechnol.* **10**, 209-220 (2015).
- [56] Y. W. Oh, S. Chris Baek, Y. M. Kim, H. Y. Lee, K. D. Lee, C. G. Yang, E. S. Park, K. S. Lee, K. W. Kim, G. Go, J. R. Jeong, B. C. Min, H. W. Lee, K. J. Lee, and B. G. Park, Field-free switching of perpendicular magnetization through spin-orbit torque in antiferromagnet/ferromagnet/oxide structures, *Nat. Nanotechnol.* **11**, 878-884 (2016).
- [57] S. Sahoo, T. Mukherjee, K. D. Belashchenko, and Ch. Binek, Isothermal low-field tuning of exchange bias in epitaxial Fe/Cr<sub>2</sub>O<sub>3</sub>/Fe, *Appl. Phys. Lett.* **91**, 172506 (2007).
- [58] Y. Shiratsuchi, K. Wakatsu, T. Nakamura, H. Oikawa, S. Maenou, Y. Narumi, K. Tazoe, C. Mitsumata, T. Kinoshita, H. Nojiri, and R. Nakatani, *Appl. Phys. Lett.* **100**, 262413 (2012).
- [59] D. Mergel, H. Heitmann, and P. Hansen, Pseudocrystalline model of the magnetic anisotropy in amorphous rare-earth-transition-metal thin films, *Phys. Rev. B* **47**, 882-891 (1993).
- [60] K. Chen, D. Lott, F. Radu, F. Choueikani, E. Otero, and P. Ohresser, Temperature-dependent magnetic properties of ferrimagnetic DyCo<sub>3</sub> alloy films, *Phys. Rev. B* **91**, 024409 (2015).
- [61] A. Agui, M. Mizumaki, T. Asahi, J. Sayama, K. Matsumoto, T. Morikawa, T. Matsushita, T. Osaka, and Y. Miura, Incident angle dependence of MCD at the Dy M<sub>5</sub>-edge of perpendicular magnetic Dy<sub>x</sub>Co<sub>100-x</sub> films, *J. Alloys Compd.* **408-412**, 741 (2006).

- [62] A. Agui, M. Mizumaki, T. Asahi, K. Matsumoto, T. Morikawa, J. Sayama, and T. Osaka, Microscopic magnetic property of perpendicular magnetic films of  $\text{Dy}_x\text{Co}_{100-x}$  measured using soft X-ray magnetic circular dichroism, *J. Phys. Chem. Solids*. **68**, 2148 (2007).
- [63] V. Lauter, H. Ambaye, R. Goyette, W.-T. H. Lee, and A. Parizzi, Highlights from the magnetism reflectometer at the SNS, *Physica B: Condens. Matter*. **404**, 2543 (2009).
- [64] L. G. Parratt, Surface Studies of Solids by Total Reflection of X-Rays, *Phys. Rev.* **95**, 359 (1954).
- [65] V. A. Sereдкин, G. I. Frolov, and V. Yu. Yakovchuk, One-directional magnetic anisotropy in NiFe/TbFe layered film structure, *Sov. Tech. Phys. Lett.* **9**, 621(1983).
- [66] V. A. Sereдкин, S. V. Stolyar, G. I. Frolov and V. Yu. Yakovchuk, Thermomagnetic data writing and erasing in DyCo/NiFe (TbFe/NiFe) film structures, *Tech. Phys. Lett.* **30**, 820-822 (2004).
- [67] D. H. Kim, M. Haruta, H. W. Ko, G. Go, H. J. Park, T. Nishimura, D. Y. Kim, T. Okuno, Y. Hirata, Y. Futakawa, H. Yoshikawa, W. Ham, S. Kim, H. Kurata, A. Tsukamoto, Y. Shiota, T. Moriyama, S. B. Choe, K. J. Lee, T. Ono, Bulk Dzyaloshinskii-Moriya interaction in amorphous ferrimagnetic alloys, *Nat Mater.* **18** 685-690 (2019).
- [68] M. Belmeguenai, J. P. Adam, Y. Roussigne, S. Eimer, T. Devolder, J. V. Kim, S. M. Cherif, A. Stashkevich, and A. Thiaville, Interfacial Dzyaloshinskii-Moriya interaction in perpendicularly magnetized Pt/Co/ $\text{AlO}_x$  ultrathin films measured by Brillouin light spectroscopy, *Phys. Rev. B* **91**, 180405 (2015).